Tensile properties of polyacrylonitrile- and pitch-based hybrid carbon fiber/polyimide composites with some nanoparticles in the matrix

Kimiyoshi Naito

Abstract The tensile properties and fracture behavior of polyacrylonitrile (PAN)- and pitch-based hybrid carbon fiber/polyimide composites with several types of nanoparticles (25 nm C, 20–30 nm β-SiC, 130 nm β-SiC, 80 nm SiO_2, and 300 nm SiO_2) added to the matrix were investigated. The tensile stress–strain curves of PAN- and pitch-based hybrid carbon fiber/polyimide composites with 25 nm C, 20–30 nm β-SiC, and 80 nm SiO_2 nanoparticles have complex shapes (jagged trace), whereas the tensile response of hybrid carbon fiber/polyimide composites with 130 nm β-SiC and 300 nm SiO_2 nanoparticles indicates an instantaneous failure. The stress after the initial failure in hybrid carbon fiber/polyimide composites improves by adding 25 nm C, 20–30 nm β-SiC, and 80 nm SiO_2 nanoparticles to the matrix and correlates with the fracture toughness of the polyimide matrix.

Introduction

Fiber-reinforced polymer matrix composites are commonly used materials in aerospace, automotive, and sporting goods industries [1, 2]. A large number of these composites are used in lightweight and/or dimensionally stabilized structural materials because of their high specific strength and modulus, and low thermal expansion; however, their use is limited to highly specialized situations in which conditions such as brittle fracture behavior arise. By mixing two or more types of fibers in a common matrix to form

K. Naito (✉)
Hybrid Materials Unit, Composite Materials Group, National Institute for Materials Science, 1-2-1 Sengen, Tsukuba 305-0047, Ibaraki, Japan
e-mail: NAITO.Kimiyoshi@nims.go.jp

hybrid fiber/polymer composites may create materials possessing the combined properties of the individual composite [3]. There have been several papers on the advantages and applications of hybrid fiber/polymer composites around 1980 [3–5]. Earlier, in 1972, Hayashi et al. [6] have discussed the tensile properties of a carbon/glass hybrid fiber/epoxy composite and proposed a hybrid-design method on the basis of the rule of mixtures. Moreover, Short et al. [7, 8], Hardaker et al. [9], and Chou et al. [10] have reviewed several hybrid fiber/polymer composites. In general, carbon/glass and carbon/aramid hybrid fiber were mainly used in previous investigations that explored the cost-effective utilization of expensive fibers by using them in hybrid fiber/polymer composites [5].

Polyacrylonitrile (PAN)- and pitch-based carbon fibers are widely used as reinforcement in carbon-fiber-reinforced polymer-matrix composites because of their high specific strength and modulus [11–13]. The development of carbon fibers has been advancing in two directions: high-strength fibers with very high tensile strength and adequately high strain-to-failure (approximately 2 %) and high-modulus fibers with very high stiffness. Today, several high tensile strength PAN-based (more than 6 GPa) and high-modulus pitch-based (more than 900 GPa) carbon fibers are commercially available [11, 14–16]. Thus, high-performance PAN- and pitch-based hybrid carbon fiber/polymer composites may be created.

In various industrial applications, polymer-matrix composites should have a high-temperature range. Polyimides are one of the most important subsets of high-performance and -temperature polymers that have been used as coatings, matrices for composites, and adhesives in the aerospace industry due to their excellent thermo-oxidative stability, high glass-transition temperature, radiation resistance, and mechanical properties [17, 18].

Fig. 1 Chemistry of Skybond 703
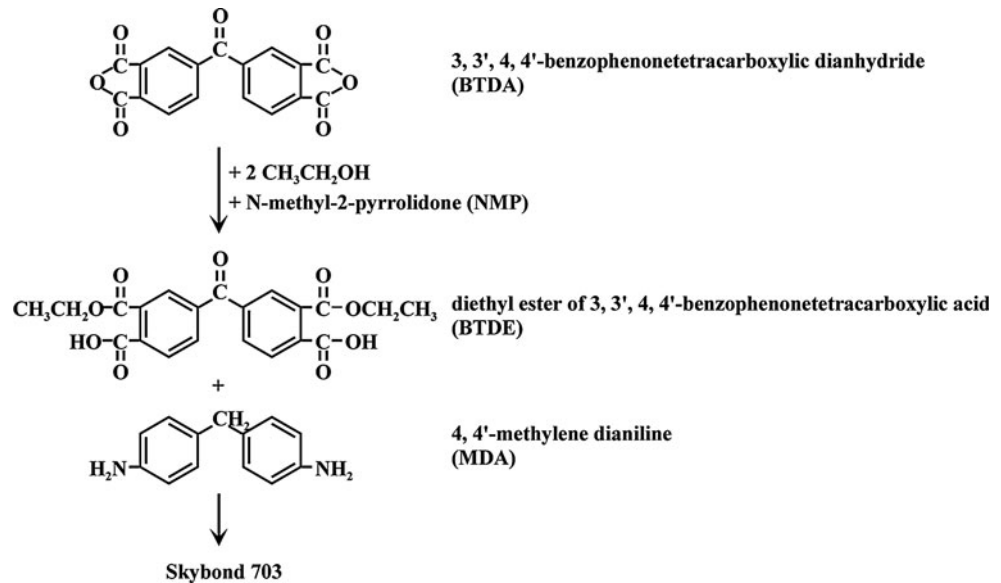
Extensive research and development of fiber-reinforced polymer-matrix composites has led to a remarkable performance improvement of the system, which exhibits excellent in-plane properties. Another critical deficiency in structural composites is the presence of matrix-rich regions in the gaps between the laminates [19]. These regions, in which cracks easily initiate and propagate, are difficult to reinforce with traditional microscale reinforcements. Nanostructure-filled polymers can be utilized to produce fiber-reinforced polymer-matrix composites because they can be strained out by the small gaps between the fibers. Various nanoscale materials (nano-Al_2O_3 [20], nanoclay [21–23], carbon nanotube [24, 25], carbon nanofiber [26, 27], nano-SiO_2 [28], graphite nanoplatelet [29], fullerene [30, 31]) were explored to selectively reinforce the matrix-rich regions.

In this study, high tensile-strength PAN-based and high-modulus pitch-based hybrid carbon fiber/polyimide composites with several types of nanoparticles (25 nm C, 20–30 nm β-SiC, 130 nm β-SiC, 80 nm SiO_2, and 300 nm SiO_2) added to the matrix were prepared. In addition, the tensile properties and fracture behavior of these hybrid carbon fiber/polyimide composites were investigated.

Experimental procedure

Materials

High tensile-strength PAN-based (T1000GB: T1000GB-12000-40D) and high-modulus pitch-based (K13D: K13 D2U) carbon fibers were used in this study. The T1000GB PAN-based carbon fiber and K13D pitch-based carbon fiber were supplied by Toray Industries, Inc. and

Mitsubishi Plastics, Inc., respectively, as a large group of carbon fiber filaments packaged together in a single spool also referred to as a roving or strand. The term "T1000GB-12000-40D" refers to the T1000GB carbon-fiber bundle that contains 12,000 (12 K) filaments, and the weight of a strand per 1000 m, Tex, is 485 g/1000 m. "K13D2U" refers to the K13D carbon-fiber bundle that contains 2,000 (2 K) filaments, and Tex is 365 g/1000 m. The specific density and tensile modulus of the T1000GB PAN-based and K13D pitch-based carbon fibers are 1.80 g/cm³ and 294 GPa, and 2.20 g/cm³ and 935 GPa, respectively [14–16].[1] The as-received fibers were subjected to commercial surface treatment and sizing (epoxy compatible sizing).

The polyimide used in this study was prepared from a commercially available polyimide precursor [PAA: poly(amic acid)] solution (Skybond 703, Industrial Summit Technology Co.). The chemistry of Skybond 703 is shown in Fig. 1. First, 3,3′,4,4′-benzophenonetetracarboxylic dianhydride was prereacted with ethanol using N-methyl-2-pyrrolidone (NMP) as the solvent, and then, 4,4′-methylene dianiline was added [32]. The specific density of the polyimide is 1.17 g/cm³.[2]

Five different types of nanoparticles (25 nm C, 20–30 nm β-SiC, 130 nm β-SiC, 80 nm SiO_2, and 300 nm SiO_2) were used. The 25 nm C nanoparticles (#5500) was supplied by Tokai Carbon Corp. The 20–30 nm β-SiC,

---

[1] These values were obtained from the producer's data sheet. The tensile modulus of the T1000GB PAN-based and K13D pitch-based carbon fibers were measured using a single filament tensile test at a gauge length of 25 mm, and they were 291 ± 11 and 940 ± 48 GPa, respectively [14].

[2] This value was obtained from the producer's data sheet. The specific density of the bulk polyimide without nanoparticles measured via ethanol immersion (ASTM D792) [33] was 1.297 g/cm³ [34].

130 nm β-SiC, and 80 nm SiO$_2$ nanoparticles were supplied by Nanostructured & Amorphous Materials, Inc., and the 300 nm SiO$_2$ nanoparticles (SE1050) were supplied by Admatecs Company Limited. All the as-received nanoparticles were not subjected to surface treatment. The shapes of 25 nm C, 130 nm β-SiC, and 300 nm SiO$_2$ nanoparticles are spherical, whereas those of 80 nm SiO$_2$ and 20–30 nm β-SiC nanoparticles are nearly spherical.[3] The average diameters of the 25 nm C, 20–30 nm β-SiC, 130 nm β-SiC, 80 nm SiO$_2$, and 300 nm SiO$_2$ nanoparticles are 25, 20–30, 130, 80, and 300 nm, respectively.[3] The specific densities of the C, β-SiC, and SiO$_2$ nanoparticles are 2.00, 3.22, and 2.40 g/cm^3, respectively [34].

Specimen preparation

PAN- and pitch-based hybrid carbon fiber/polyimide composites with the nanoparticles added to the matrix were prepared in three steps, which includes the preparation of a polyimide-precursor solution containing the nanoparticles, the permeation of the polyimide-precursor solution into dry laminates via vacuum-assisted resin-transfer molding (VaRTM) [35], followed by thermal imidization to produce hybrid carbon fiber/polyimide composites. In the first step, the appropriate amounts of nanoparticles and 20 wt% NMP were added to a polyimide precursor solution (Skybond 703). This solution was prepared by simultaneously rotating and revolving using a rotation/revolution mixer (AR-250, Thinky Co. Ltd.) under the following driving conditions: mixing mode (rotation: 800 rpm and revolution: 2000 rpm) for 10 min and defoaming mode (rotation: 60 rpm and revolution: 2200 rpm) for 5 min. The precursor was degassed in a vacuum oven at 90 ± 10 °C for 1 h to remove the excess solvent. The volume fraction of all nanoparticles, V_p, was 5 vol%. In the second step, an appropriate amount of the precursor solution was allowed to permeate into the dry laminates. The dry laminates were fabricated using a tension-controlled filament-winding machine (a cube mandrel was used). The distance between the bundles was controlled to obtain the appropriate fiber-area weight (FAW). In this study, the FAWs of the T1000GB and K13D layers were 204 and 166 g/m^2, respectively. After winding, the dry laminates were prepared by fixing both edges on a flame holder (made of glass fiber/polyimide composite) with a high-viscosity instant cyanoacrylate adhesive to keep the bundles straight and parallel. Finally, the dry laminates were cut perpendicular to the fiber axis at both ends. The fiber orientations of the individual (T1000GB and K13D) carbon fiber/polyimide

and hybrid (T1000GB and K13D) carbon fiber/polyimide composites were set to [0]$_8$ and [0$_{(T1000GB)}$/0$_{(K13D)}$]$_{2S}$, respectively (the T1000GB and K13D unidirectional layers were alternately and symmetrically laminated). The number of layers in both the individual carbon fiber/polyimide and hybrid carbon fiber/polyimide composites was eight plies. The laminates were fabricated via VaRTM. Next, the individual carbon fiber/polyimide and hybrid carbon fiber/polyimide sheets were dried in a vacuum oven at 90 ± 10 °C for 8 h to remove the remaining solvent. In the third step, the individual carbon fiber/polyimide and hybrid carbon fiber/polyimide sheets were combined with silicone-coated 1165 style fiberglass peel plies (Bleeder Lease E, Airtech International Inc.) and a thin polytetrafluoroethylene release film (WL5900 0.001, Airtech International Inc.), and then, they were placed in a thin polyimide vacuum-bagging film (Thermalimide 0.002, Airtech International Inc.). The contents were compressed up to 0.7 MPa in an autoclave (ACA Series, Ashida Mfg. Co., Ltd.) and heated to 343 °C gradually. Figure 2 shows the temperature, vacuum pressure, and pressure profiles in the autoclave reactor as a function of time. To remove the residual solvent and soften the polyimides, they were heated at 120, 160, and 200 °C. To cure the polyimides completely for imidization, the materials were heated at 260, 315, and 343 °C.

The specific densities of the bulk polyimides with and without nanoparticle were measured via ethanol immersion (ASTM D792) [33], and the specific densities of polyimides with and without nanoparticles (25 nm C, 20–30 nm β-SiC, 130 nm β-SiC, 80 nm SiO$_2$, and 300 nm SiO$_2$) are 1.332, 1.408, 1.409, 1.363, 1.368, and 1.297 g/cm^3, respectively. These values, except for the polyimide with 300 nm SiO$_2$ nanoparticles, were similar to those in a
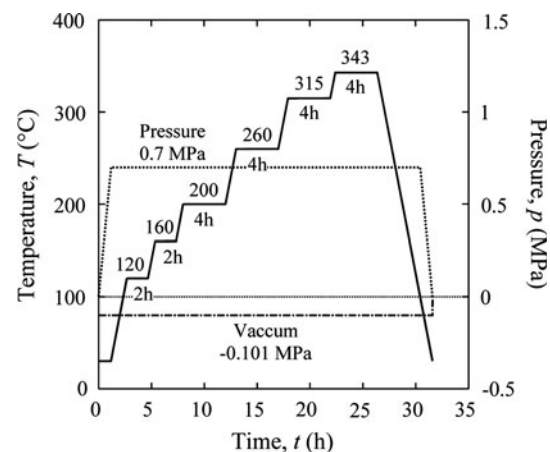

Fig. 2 Temperature, vacuum pressure, and pressure profiles as a function of time

---

[3] Producer's data sheet. The diameters of all nanoparticles were also measured using a high-magnification transmission electron microscope (TEM) (JEM 2000, JEOL) at an operating voltage of 200 kV.

previous investigation [34]. The volume fraction of all nanoparticles was 5 vol%. All individual carbon fiber/ polyimide and hybrid carbon fiber/polyimide composites were also measured via ethanol immersion [33]. The fiber volume fraction was calculated according to ASTM D3171 [36]. The fiber volume fractions of individual carbon fiber/ polyimide and hybrid carbon fiber/polyimide composites were 50 vol% (for the hybrid carbon fiber/polyimide composite: T1000GB fiber: 24.9 vol%, K13D fiber: 25.1 vol%, and T1000GB fiber/polyimide composite: K13D fiber/polyimide composite = 49.8:50.2).

The laminates were cut into rectangular pieces with straight sides and with length (gauge length, L of 100 mm), width, and thickness[4] equal to 200, 10, and approximately 1.5 mm, respectively, for tensile testing. The fiber axes were oriented in line with the length of the tensile test specimens (fiber orientation 0° specimen). To eliminate the effect of stress concentration due to the surface roughness of the edges, the edges of the tensile test specimens were slightly polished to remove deep scratches. Thinner, plain, woven fabric glass-fiber-reinforced plastics (50 mm in length, 10 mm in width, and 1 mm in thickness) with tapered tabs were affixed to the tensile test specimens to minimize the damage from the grips that secured the specimens in the specimen fixture (tensile-testing machine).

Observation

The morphology of individual carbon fiber/polyimide and hybrid carbon fiber/polyimide composites was observed using a digital microscope, and the dispersion of nano-particles was examined with a transmission electron microscope (TEM) (JEM 2000, JEOL) at an operating voltage of 200 kV.

Tensile test

The tensile tests of individual carbon fiber/polyimide and hybrid carbon fiber/polyimide composite specimens were conducted using a universal testing machine (Autograph AG-series, Shimadzu) with a load cell and crosshead speed of 100 kN and 5.0 mm/min, respectively. All tests were conducted in a laboratory at 23 ± 3 °C and 50 ± 5 % relative humidity. Strain gauges were used to measure longitudinal strains. Six samples of each composite were tested. Tensile modulus was calculated from the elastic region of the stress–strain curves using the least-squares method.

---

[4] The thickness of individual (T1000GB and K13D) and hybrid carbon fiber/polyimide composites was similar at approximately 1.5 mm.

Results

Morphology and dispersion of nanoparticles

Figure 3 shows the digital micrograph of the morphology of PAN- and pitch-based hybrid carbon fiber/polyimide composites without nanoparticles. The fabrication of polyimide composites is difficult because they produce volatiles during chemical reactions. In addition, volatiles are produced from the residual solvent during curing. Because aromatic polyimides are insoluble and infusible, a polyimide precursor consisting of PAA in a high-boiling polar solvent such as NMP is used to decrease the viscosity of polyimides. PAA is converted into polyimide through curing, and the volatilization of solvents and by-products creates voids in polyimide composites [37, 38]. However, there were no visible microsized voids in the cross-sectional view of hybrid carbon fiber/polyimide composite, as shown in Fig. 3. The content of the residual solvent in a composite should be controlled to avoid the presence of voids. Similar results were observed in individual carbon fiber/polyimide composites with and without nanoparticles and hybrid carbon fiber/polyimide composites with nano-particles. Individual carbon fiber/polyimide and hybrid carbon fiber/polyimide composites could be fabricated using rotation/revolution mixing, VaRTM, and autoclave curing.

The TEM specimens of polyimides with 25 nm C, 20–30 nm β-SiC, 130 nm β-SiC, and 80 nm SiO_2 nano-particles were removed by cutting the epoxy-molded blocks containing nanoparticle-filled polyimides protruding from the laminates using a diamond knife. A TEM specimen of polyimide with 300 nm SiO_2 nanoparticles was cut directly from the laminate within the K13D fiber/polyimide
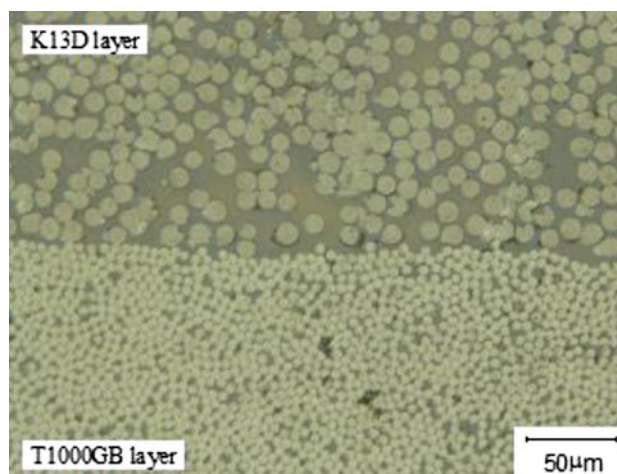

Fig. 3 Cross-sectional view of the T1000GB PAN-based and K13D pitch-based hybrid carbon fiber/polyimide composites without nanoparticles

composite layer using a focused ion beam (Strata DB235M, FEI). Thin sections with a thickness of <100 nm were collected on a copper grid. Figure 4 shows the TEM images of nanoparticles dispersed in polyimides. Most of the nanoparticles tend to aggregate. Especially, the smaller nanoparticles (25 nm C and 20–30 nm β-SiC) show a strong aggregation trend. Under low magnification, approximately 300 nm large aggregates of non-compact 25 nm C and 20–30 nm β-SiC nanoparticles were observed, whereas the size of the aggregates of the 80 nm SiO_2 nanoparticles was approximately 500 nm. The diameter of the individual 300 nm SiO_2 nanoparticles was approximately 300 nm although large diameter differences among the particles were observed with TEM because of the distribution trend of 300 nm SiO_2 nanoparticles and the TEM sample slice (<100 nm). Higher magnification revealed that the sizes of the individual 25 nm C, 20–30 nm β-SiC, 130 nm β-SiC, and 80 nm SiO_2 nanoparticles were approximately 25, 20–30, 130, and 80 nm, respectively. The nonuniform dispersion and trend of the degree of aggregation of the nanoparticles in polyimides were mainly due to the aggregate nature of the nanoparticles resulting from their large specific-surface area and high surface energy.

In a previous investigation [34], using TEM, we examined the dispersion of nanoparticles in nanoparticle-filled
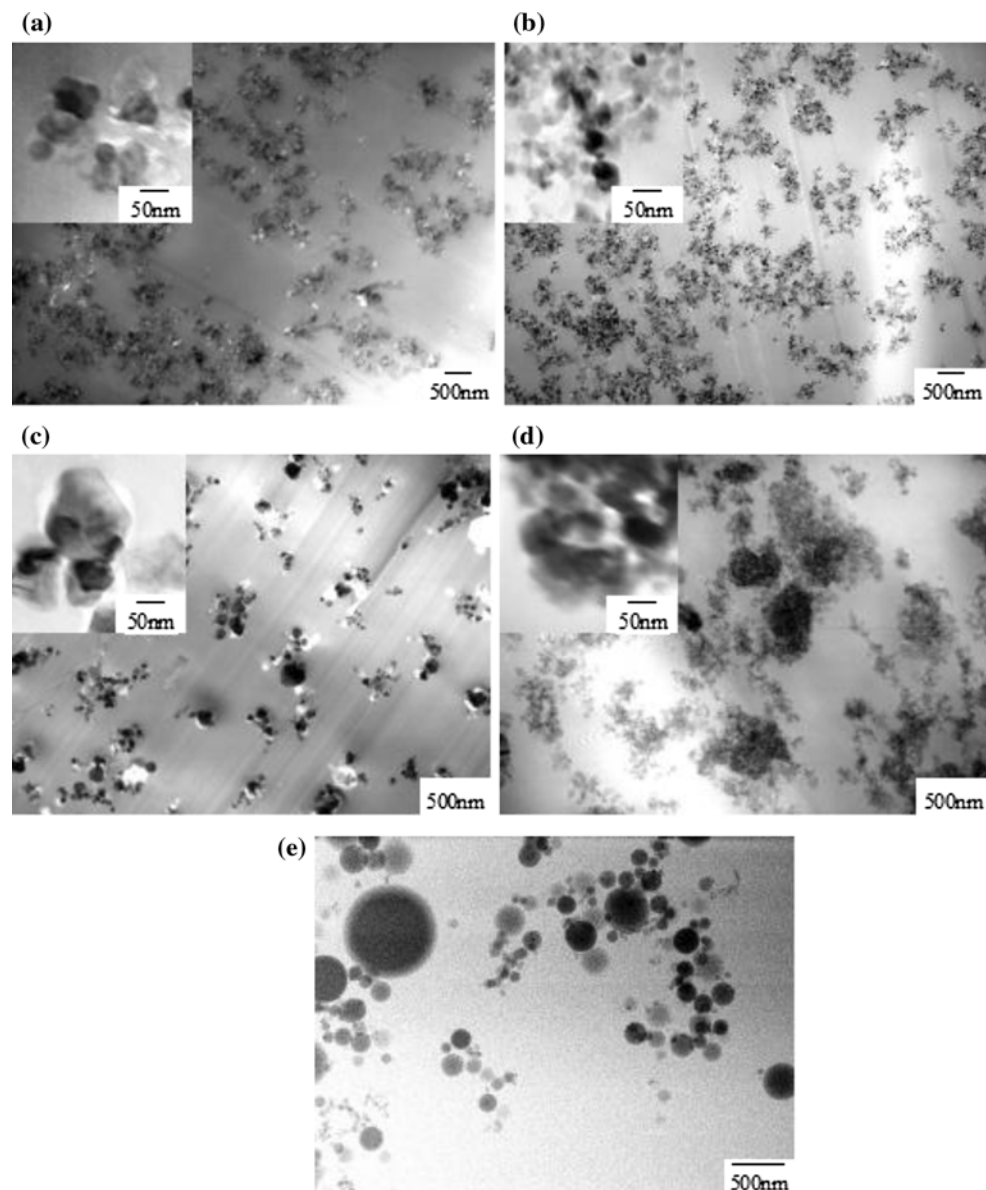

Fig. 4 TEM images of polyimides with nanoparticles: a 25 nm C nanoparticle, b 20–30 nm β-SiC nanoparticle, c 130 nm β-SiC nanoparticle, d 80 nm SiO_2 nanoparticle, and e 300 nm SiO_2 nanoparticle

polyimides (25 nm C, 20–30 nm β-SiC, 130 nm β-SiC, 10 nm SiO$_x$ (x = 1.2–1.6), 80 nm SiO$_2$, 11 nm γ-Al$_2$O$_3$, and 40–80 nm γ-Al$_2$O$_3$) with the four different volume fractions of nanoparticles (V_p = 0.5, 1, 5, and 10 vol%); we found that the dispersion of nanoparticles improved at high volume fractions (V_p = 5, 10 vol%).

Tensile properties

Figure 5 shows the typical tensile stress–strain (σ–ε) curves for T1000GB and K13D hybrid carbon fiber/polyimide composites with and without nanoparticles. In addition, the

stress–strain curves of individual (T1000GB and K13D) carbon fiber/polyimide with and without nanoparticles are shown in these figures.

In individual carbon fiber/polyimide with and without nanoparticles, the applied stress was approximately linearly proportional to strain up to failure. At this point, modulus, strength, and failure strain are defined as tensile modulus, E_C, tensile strength, σ_{Cf}, and failure strain, ε_{Cf}, respectively.

In T1000GB and K13D hybrid carbon fiber/polyimide composites with and without nanoparticles (25 nm C, 20–30 nm β-SiC, and 80 nm SiO$_2$), the tensile stress–strain

Fig. 5 Typical tensile stress–strain curves of individual carbon fiber/polyimide and hybrid carbon fiber/polyimide composites: **a** without nanoparticles, **b** 25 nm C nanoparticles, **c** 20–30 nm β-SiC nanoparticles, **d** 130 nm β-SiC nanoparticles, **e** 80 nm SiO$_2$ nanoparticles, and **f** 300 nm SiO$_2$ nanoparticles
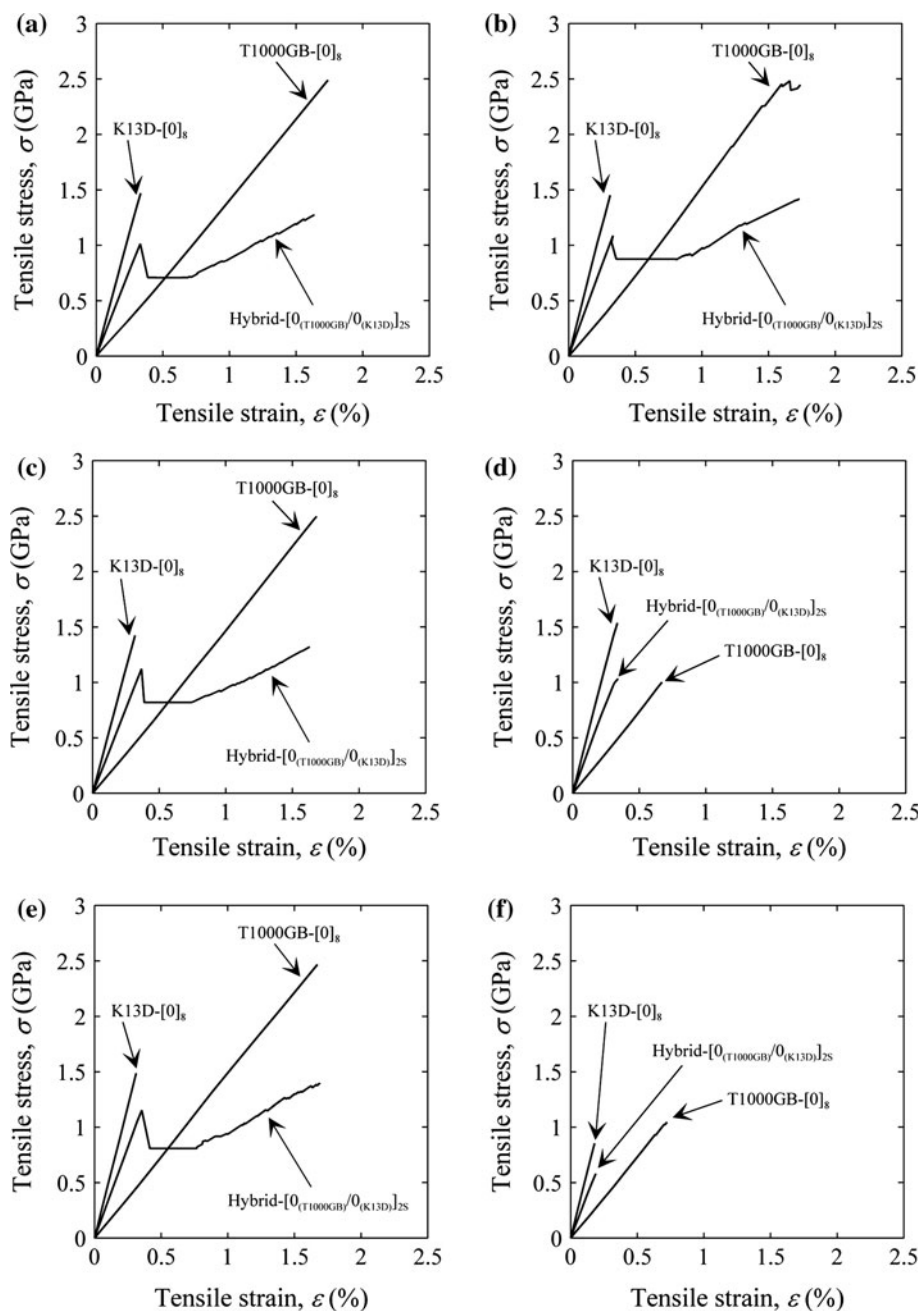
curves have a complex shape (jagged trace). The applied stress is approximately linearly proportional to strain and then considerably decreases at the failure of the high-modulus K13D fiber/polyimide composite layers. Stress increased with increasing strain but the modulus reduced because of the transfer of stress from the broken K13D to the high-strength T1000GB fiber/polyimide composite layers. Finally, catastrophic failure occurred in the T1000GB fiber/polyimide composite layers. In the high-modulus K13D fiber/polyimide composite layers, the hybrid fiber/polyimide composite shows an intermediate modulus during the initial stage of loading (tensile modulus, E_C). Subsequently, when the K13D fiber/polyimide composite layers started failing (at this point, strength, and strain are defined as the initial fracture strength, σ_{Ci}, and initial failure strain, ε_{Ci}, respectively), the high-strength T1000GB fiber/polyimide composite layers sustained the load (stress) and the hybrid carbon fiber/polyimide composite sustained high loads without instantaneous failure (this modulus was defined as the secondary tensile modulus, E_C^*). The holding stress level, σ_{Ch}, is different among various nanoparticles (25 nm C, 20–30 nm β-SiC, and 80 nm SiO_2). Finally, the hybrid fiber/polyimide composite fractured at maximum load. At this point, strength and strain were defined as the tensile strength, σ_{Cf}, and failure strain, ε_{Cf}, respectively.

However, for hybrid carbon fiber/polyimide composites with 130 nm β-SiC and 300 nm SiO_2 nanoparticles, the tensile stress–strain curve does not have a complex shape and only initial fracture is observed. At this point modulus, strength, and strain are defined as the tensile modulus, E_C, fracture strength, σ_{Cf}, and failure strain, ε_{Cf}, respectively.

Figure 6 shows the tensile stress–strain curves of individual carbon fiber/polyimide and hybrid carbon fiber/
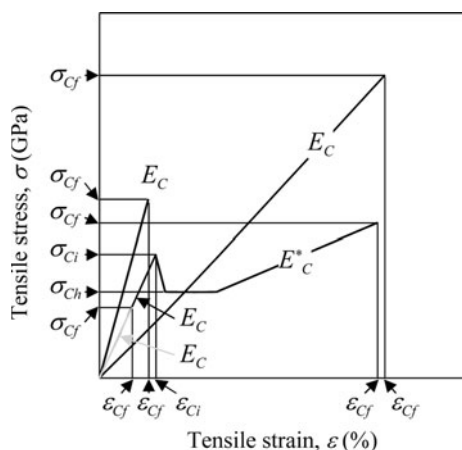

Fig. 6 Typical tensile stress–strain curves for individual carbon fiber/polyimide and hybrid carbon fiber/polyimide composites and the definitions of modulus, strength, stress, and strain

polyimide composites and the definitions of modulus (E_C, E_C^*), strength (σ_{Ci}, σ_{Cf}), stress (σ_{Ch}), and strain (ε_{Ci}, ε_{Cf}).

Table 1 summarizes tensile modulus, tensile strength, failure strain, secondary tensile modulus, initial fracture strength, initial failure strain, and holding stress. The results show that the tensile modulus of individual (T1000GB and K13D) fiber/polyimide with nanoparticles is similar to that of individual carbon fiber/polyimide without nanoparticles. Moreover, the tensile strength and failure strain of individual carbon fiber/polyimide with 25 nm C, 20–30 nm β-SiC, and 80 nm SiO_2 nanoparticles are similar to those of individual carbon fiber/polyimide without nanoparticles. However, the tensile strength and failure strain of T1000GB fiber/polyimide composites with 130 nm β-SiC and 300 nm SiO_2 nanoparticles are relatively lower than those of T1000GB fiber/polyimide composites without nanoparticles. The tensile strength and failure strain of the K13D fiber/polyimide composite with 130 nm β-SiC nanoparticles are similar to those of the K13D fiber/polyimide composite without nanoparticles. However, the tensile strength and failure strain of the K13D fiber/polyimide composite with 300 nm SiO_2 nanoparticles are lower than those of the K13D fiber/polyimide composite without nanoparticles.

Hybrid carbon fiber/polyimide composites with and without nanoparticles (25 nm C, 20–30 nm β-SiC, and 80 nm SiO_2) have similar tensile modulus, secondary tensile modulus, initial fracture strength, initial failure strain, tensile strength, and failure strain. For hybrid carbon fiber/polyimide composites with 130 nm β-SiC and 300 nm SiO_2 nanoparticles, tensile strength, and failure strain are relatively lower than those of hybrid carbon fiber/polyimide composites without nanoparticles.

The initial failure strain of hybrid carbon fiber/polyimide composites with and without nanoparticles (25 nm C, 20–30 nm β-SiC, and 80 nm SiO_2) is 11 % higher than the corresponding failure strain of K13D fiber/polyimide composites. Moreover, the final failure strain of hybrid carbon fiber/polyimide composites with and without nanoparticles (25 nm C, 20–30 nm β-SiC, and 80 nm SiO_2) is similar to that of T1000GB fiber/polyimide composites. For hybrid carbon fiber/polyimide composites with 130 nm β-SiC and 300 nm SiO_2 nanoparticles, failure strain is slightly (3–5 %) higher than that of K13D fiber/polyimide composites with these nanoparticles. However, for the hybrid carbon fiber/polyimide composite with 300 nm SiO_2 nanoparticles, failure strain (also tensile strength) is relatively low compared with that of the K13D fiber/polyimide and hybrid carbon fiber/polyimide composites with and without the rest of the nanoparticles.

Figure 7 shows the fracture features of hybrid carbon fiber/polyimide composites with and without nanoparticles.

Table 1 Tensile properties of the individual carbon fiber/polyimide and hybrid carbon fiber/polyimide composites

	Tensile modulus E_C (GPa)	Initial fracture strength σ_{Ci} (GPa)	Initial failure strain ε_{Ci} (%)	Secondary tensile modulus E_C^* (GPa)	Tensile strength σ_{Cf} (GPa)	Failure strain ε_{Cf} (%)	Holding stress σ_{Ch} (GPa)
Unfilled							
T1000GB	144 (1)	–	–	–	2.466 (0.033)	1.724 (0.020)	–
K13D	455 (7)	–	–	–	1.453 (0.027)	0.322 (0.009)	–
Hybrid	309 (4)	1.065 (0.041)	0.348 (0.016)	71 (2)	1.246 (0.021)	1.682 (0.032)	0.722 (0.022)
25 nmC nanoparticle filled							
T1000GB	148 (1)	–	–	–	2.540 (0.054)	1.714 (0.019)	–
K13D	456 (12)	–	–	–	1.388 (0.046)	0.309 (0.004)	–
Hybrid	317 (8)	1.088 (0.002)	0.342 (0.006)	74 (3)	1.423 (0.011)	1.675 (0.041)	0.861 (0.013)
20–30 nm β SiC nanoparticle filled							
T1000GB	147 (1)	–	–	–	2.536 (0.028)	1.693 (0.010)	–
K13D	450 (4)	–	–	–	1.393 (0.029)	0.313 (0.005)	–
Hybrid	312 (9)	1.083 (0.036)	0.351 (0.012)	71 (3)	1.295 (0.019)	1.674 (0.032)	0.819 (0.002)
130 nm β-SiC nanoparticle filled							
T1000GB	146 (1)	–	–	–	0.992 (0.012)	0.656 (0.012)	–
K13D	458 (8)	–	–	–	1.431 (0.075)	0.319 (0.013)	–
Hybrid	321 (5)	–	–	–	1.034 (0.008)	0.334 (0.006)	–
80 nm SiO$_2$ nanoparticle filled							
T1000GB	145 (2)	–	–	–	2.441 (0.020)	1.689 (0.014)	–
K13D	453 (12)	–	–	–	1.413 (0.056)	0.310 (0.004)	–
Hybrid	322 (4)	1.122 (0.024)	0.352 (0.003)	74 (1)	1.358 (0.029)	1.672 (0.014)	0.808 (0.006)
300 nm SiO$_2$ nanoparticle filled							
T1000GB	146 (2)	–	–	–	1.058 (0.013)	0.721 (0.009)	–
K13D	456 (15)	–	–	–	0.823 (0.021)	0.182 (0.001)	–
Hybrid	314 (9)	–	–	–	0.581 (0.009)	0.188 (0.002)	–

() indicate standard deviations

Fig. 7 Fracture features of hybrid carbon fiber/polyimide composites with and without nanoparticles: **a** without nanoparticles, **b** 25 nm C nanoparticles, **c** 20–30 nm β-SiC nanoparticles, **d** 130 nm β-SiC nanoparticles, **e** 80 nm SiO$_2$ nanoparticles, and **f** 300 nm SiO$_2$ nanoparticles
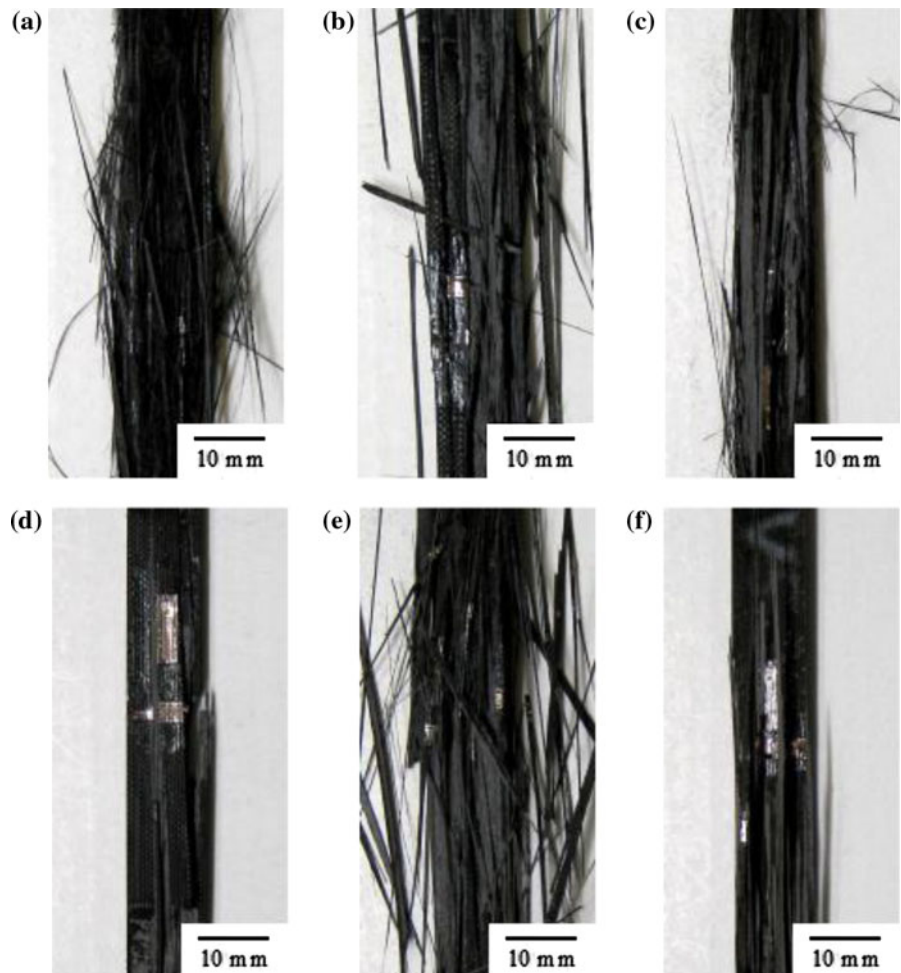
Splitting fractures were observed in hybrid carbon fiber/polyimide composites with and without nanoparticles (25 nm C, 20–30 nm β-SiC, and 80 nm SiO$_2$). However, large splitting fractures were not observed in hybrid carbon fiber/polyimide composites with 130 nm β-SiC and 300 nm SiO$_2$ nanoparticles, and the specimens were broken into two pieces.

During tensile tests, a charge-coupled device camera mounted on a digital microscope (Keyence, VHX-1000 and VH-Z100) allowed the real-time through-thickness-sectional view observations of the initial fracture stage of hybrid carbon fiber/polyimide composites. Figure 8 shows a digital micrograph of the through-thickness-edge-sectional view of the initial fracture stage of hybrid carbon fiber/polyimide composites without nanoparticles. Similar fracture behavior was observed in hybrid carbon fiber/polyimide composites with 25 nm C, 20–30 nm β-SiC, and 80 nm SiO$_2$ nanoparticles. For hybrid carbon fiber/polyimide composites with and without these nanoparticles, the principal transverse crack related to high-modulus fibers runs across the entire width and thickness of the K13D fiber/polyimide composite layers (white arrow in Fig. 8).

Delamination cracks are produced at the intersection of transverse cracks and T1000GB fiber/polyimide composite layers and propagate along the length near the interface between the K13D and T1000GB fiber/polyimide composite layers (black arrows in Fig. 8). Small delamination
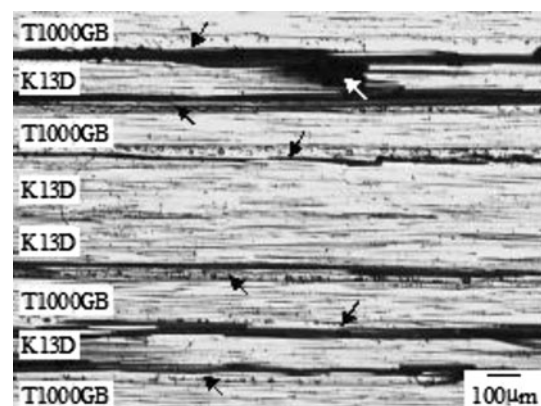

Fig. 8 Typical through-thickness-edge-section digital micrograph of the initial fracture stage of hybrid carbon fiber/polyimide composites without nanoparticles

cracks were observed in the hybrid carbon fiber/polyimide composite with 130 nm β-SiC nanoparticles. However, delamination cracks were not observed in the through-thickness-edge-sectional view of hybrid carbon fiber/polyimide composites with 300 nm SiO$_2$ nanoparticles.

Discussion

Tensile modulus

In a previous investigation [34], the tensile modulus of bulk polyimides with and without 25 nm C, 20–30 nm β-SiC, 130 nm β-SiC, and 80 nm SiO$_2$ nanoparticles was examined using the bog-bone type tensile test and was estimated to 4.18 ± 0.06, 4.65 ± 0.03, 4.83 ± 0.02, 4.42 ± 0.05, and 3.77 ± 0.04 GPa, respectively. The tensile modulus of bulk polyimide nanocomposites was improved with the addition of nanoparticles. However, in this study, the tensile modulus of individual (T1000GB and K13D) and hybrid carbon fiber/polyimide composites was improved slightly, or not at all, with the addition of nanoparticles, as shown in Table 1. The tensile modulus of individual and hybrid carbon fiber/polyimide composites, E_C was calculated using the simple rule of mixtures,

$$E_C = E_f V_f + E_m V_m \tag{1}$$

in which E_f, E_m, V_f, and V_m are the tensile modulus and volume fractions of fiber and matrix, respectively. The tensile modulus of individual (T1000GB and K13D) and hybrid carbon fiber were 291, 940 [14], and 617 (T1000GB fiber: K13D fiber = 49.8:50.2) GPa, respectively. The values predicted from the rule of mixtures with and without 25 nm C, 20–30 nm β-SiC, 130 nm β-SiC, and 80 nm SiO$_2$ nanoparticles are ranging from 147 to 148 (T1000GB), 472 (K13D) and 310–311 (hybrid) GPa, respectively. The influence of the addition of nanoparticles on the tensile modulus could not be observed. The individual and hybrid carbon fiber/polyimide composites show fiber-dominated behavior of the tensile modulus in the plane of the fiber reinforcements.

The tensile and secondary tensile moduli of hybrid carbon fiber/polyimide composites were also calculated using the simple rule of mixtures,

$$E_{C(Hybrid)} = E_{C(T1000GB)} V_{T1000GB} + E_{C(K13D)} V_{K13D} \text{ (for tensile modulus)} \tag{2}$$

$$E^*_{C(Hybrid)} = E_{C(T1000GB)} V_{T1000GB} \text{ (for secondary modulus)} \tag{3}$$

in which $V_{T1000GB}$ and V_{K13D} are the volume fractions of T1000GB and K13D carbon fiber/polyimide composites, respectively. The estimated tensile and secondary tensile

moduli of hybrid carbon fiber/polyimide composites were 301 and 73 GPa, respectively. The values predicted from the rule of mixtures and the experimental results ($E_C = 316$, $E^*_C = 73$ GPa) are in good agreement. Similar results were observed for hybrid fiber/polymer composites as those reported in [39–41].

Tensile strength and failure strain

The tensile and initial fracture strengths of hybrid carbon fiber/polyimide composites with and without 25 nm C, 20–30 nm β-SiC, and 80 nm SiO$_2$ nanoparticles were also calculated using the rule of mixtures.

$$\sigma_{Ci(Hybrid)} = \sigma_{Cf(K13D)} V_{K13D} + \varepsilon_{Cf(K13D)} E_{C(T1000GB)} \times V_{T1000GB} \text{ (for initial fracture strength)} \tag{4}$$

$$\sigma_{Cf(Hybrid)} = \sigma_{Cf(T1000GB)} V_{T1000GB} \text{ (for tensile strength)} \tag{5}$$

The estimated tensile strength, σ_{Cf}, and initial fracture strength, σ_{Ci}, of hybrid carbon fiber/polyimide composites were 1.244 and 0.939 GPa, respectively. The differences between the calculated and experimental results for the tensile and initial fracture strengths were 7 and 16 %, respectively. The experimental tensile strengths agree with those predicted by the rule of mixtures. In addition, the final failure strain, ε_{cf}, as shown in Table 1, is approximately equal to that of T1000GB fiber/polyimide composites. However, a large difference was observed in the initial fracture strength. In addition, the initial failure strain, ε_{ci}, as shown in Table 1, is higher than the failure strain of the K13D fiber/polyimide composites. Similar results observed for hybrid fiber/polymer composites characterized by the "hybrid-effect" phenomenon are reported in [39–43]. For hybrid carbon fiber/polyimide composites, the fracture of the low-elongation K13D fiber/polyimide composite layers is impeded by the greater ductility of the high-elongation T1000GB fiber/polyimide composite layers.

Fracture behavior

The tensile stress–strain curve of hybrid carbon fiber/polyimide composites with large (130 nm β-SiC and 300 nm SiO$_2$) nanoparticles indicates brittle behavior, whereas a plateau is observed in the curve of hybrid carbon fiber/polyimide composites with small nanoparticles (25 nm C, 20–30 nm β-SiC, and 80 nm SiO$_2$). This difference is thought to be possibly attributed to the enhancement of modulus and fracture toughness of matrix, the local deformation for aggregates of nanoparticles, and the damage of the fibers due to the addition of nanoparticles.

In a previous investigation [34], the tensile modulus and fracture toughness of bulk polyimides with and without 25 nm C, 20–30 nm β-SiC, 130 nm β-SiC, and 80 nm SiO$_2$ nanoparticles was examined. The tensile modulus and fracture toughness of bulk polyimide nanocomposite with large nanoparticles (130 nm β-SiC) were higher than those with small nanoparticles and without nanoparticles. The stress concentration around the broken fibers was increased with increasing the modulus of matrix and it was difficult to propagate the delamination crack by enhancement of fracture toughness of matrix. In addition, most of the nanoparticles tend to aggregate, as shown in Fig. 4. The local deformation (local stress concentration) of matrix occurred during the tensile test. The individual and hybrid carbon fiber/polyimide composites with large nanoparticles (130 nm β-SiC and 300 nm SiO$_2$) were broken into two pieces, as shown in Fig. 7 (only hybrid composites) and indicated brittle behavior, as shown in Fig. 5d, f.

The size of the aggregates of nanoparticles was approximately 300–500 nm.[5] The aggregated nanoparticles may have contacted the fibers when the polyimides shrunk during drying and curing. The small nanoparticles could be moved easily. However, large nanoparticles were difficult to move. Therefore, the fibers were damaged. The results for the individual carbon fiber/polyimide are shown in Fig. 5d, f. The tensile strength and failure strain of the T1000GB fiber/polyimide composites with 130 nm β-SiC and 300 nm SiO$_2$ nanoparticles are lower than those of T1000GB fiber/polyimide composites with small nanoparticles and without nanoparticles. The tensile strength and failure strain of K13D fiber/polyimide composites with 300 nm SiO$_2$ nanoparticles are also lower than those of the K13D fiber/polyimide composites with small nanoparticles and without nanoparticles. However, the tensile strength and failure strain of the K13D fiber/polyimide composites with 130 nm β-SiC nanoparticles are similar to those of the K13D fiber/polyimide composites with small nanoparticles and without nanoparticles.

There are some differences between the composites with large nanoparticles due to the differences in modulus and fracture toughness of matrix, and dispersion and diameter of nanoparticles. It was found that the selection of nanoparticles was critical for preventing instantaneous failure.

This section summarizes the fracture behavior of hybrid carbon fiber/polyimide composites with and without 25 nm C, 20–30 nm β-SiC, and 80 nm SiO$_2$ nanoparticles. The applied stress is approximately linearly proportional to the strain in the initial stage of loading. The K13D fiber/polyimide composite layers start failing at the initial fracture stage. The principal transverse crack runs across the entire width and thickness of the K13D fiber/polyimide composite layers. Delamination cracks are produced at the intersection of transverse cracks and T1000GB fiber/polyimide composite layers; however, the delamination cracks do not extend over the entire length of the specimen. This results in a rapid stress reduction and slight increase in strain, as shown in Fig. 5a–c, e. Delamination cracks propagate along the length near the interface between the K13D and T1000GB fiber/polyimide composite layers, and this results in an approximately constant stress and large increase in strain, as shown in Figs. 5a–c, e. Finally, delamination cracks extend over the entire length of the specimen, so that the K13D fiber/polyimide composite layers are completely unloaded, and the final fracture considered is the fracture of the T1000GB fiber/polyimide composite layers. This results in secondary tensile modulus and failure strain, as shown in Fig. 5a–c, e.

The total delamination-energy-release rate, g_T^D, is given by the following equation [44, 45],

$$g_T^D = \frac{P^2}{2B}\frac{d\lambda}{da} \tag{6}$$

where P is the applied load with the specimen width B, and the compliance λ is obtained from the load–displacement curve ($\lambda = U/P = \varepsilon L/\sigma A$, where U is the displacement) and delamination crack length a of the hybrid carbon fiber/polyimide composite. The rearrangement of the total delamination-energy-release-rate expression (Eq. 6) gives the following equation:

$$g_T^D = \frac{\sigma^2 AL}{2B}\frac{dS_C^D}{da} \tag{7}$$

where σ is the stress applied on a specimen with area A and gauge length L (100 mm), S_C^D is the compliance obtained from the stress–strain curve estimated as follows:

$$S_C^D = \frac{1}{E_C^D} \tag{8}$$

The tensile modulus of the delamination-cracked hybrid carbon fiber/polyimide composites is also given by the rule of mixtures.

$$E_{C(Hybrid)}^D = \frac{E_{C(Hybrid)}^* \cdot a + E_{C(Hybrid)} \cdot (L-a)}{L}. \tag{9}$$

Delamination crack length is given by,

$$a = \frac{\left(E_{C(Hybrid)}^D - E_{C(Hybrid)}\right) \cdot L}{E_{C(Hybrid)}^* - E_{C(Hybrid)}} \tag{10}$$

From Eqs. (6–8), the total delamination-energy-release rate is modified accordingly as follows:

---

[5] This size is relatively smaller than the distance between each fibers related to the $V_f = 50\%$ (the distance between each fibers at $V_f = 50\%$ are similar to the diameters of each fiber).

$$g_{\mathrm{T}}^{\mathrm{D}} = \frac{\sigma^2 A L^2}{2B} \frac{E_{\mathrm{C(Hybrid)}}^* - E_{\mathrm{C(Hybrid)}}}{\left(\left(E_{\mathrm{C(Hybrid)}}^* - E_{\mathrm{C(Hybrid)}} \right) \cdot a + E_{\mathrm{C(Hybrid)}} \cdot L \right)^2}$$

(11)

In a previous investigation [46], delamination-cracked model hybrid carbon fiber/epoxy composites were fabricated by high-strength PAN-based [fiber: IM600; matrix: epoxy (133)] and high-modulus pitch-based [fiber: K13D; matrix: epoxy (HX1)] prepregs using the hand lay-up, vacuum bagging (no bleeder), and autoclave curing to examine the tensile properties and delamination crack growth in these composites. A principal transverse crack was introduced at the center of all K13D fiber/epoxy composite layers. Delamination cracks were produced and controlled using release films. Therefore, for each type of delamination-cracked model hybrid carbon fiber/epoxy composites, the stress applied to the specimens was approximately linearly proportional to the strain during the initial stage of loading. The tensile modulus, E_{C}^{D}, of these composites decreased with increasing delamination crack length, a. Then, a large increase in strain was observed at an approximately constant stress. Finally, the stress–strain curves of delamination-cracked model hybrid carbon fiber/epoxy composites show secondary tensile modulus, and the specimens failed at a similar strain. In addition, total delamination-energy-release rates were calculated using the same procedure, and the initial total delamination-energy-release rates for short delamination crack lengths ($a \leq 20$ mm) were similar (719 J/m^2).

The initial total delamination-energy-release rates could be estimated using the holding stress, σ_{Ch}, at delamination crack length, $a = 0$. The initial total delamination-energy-release rates of hybrid carbon fiber/polyimide composites with and without 25 nm C, 20–30 nm β-SiC, and 80 nm SiO$_2$ nanoparticles were calculated to be 1238 ± 75, 1160 ± 85, 1062 ± 40, and 927 ± 99 J/m^2, respectively. From the results of hybrid carbon fiber/polyimide composites, the critical total energy-release rate of the K13D fiber/polyimide composite, $g_{\mathrm{C(K13D)}}$, was estimated to be 2044 ± 152 J/m^2 and was larger than the initial total delamination-energy-release rates. For these hybrid carbon fiber/polyimide composites, delamination cracks propagated along the length when the total delamination-energy-release rate reached this value. After the initial fracture, stress improved with increase in the delamination energy-release rate.

In a previous investigation [34], the mode I fracture toughness of bulk polyimides with and without 25 nm C, 20–30 nm β-SiC, 130 nm β-SiC, and 80 nm SiO$_2$ nanoparticles was examined using the single-end-notched three-point-bending test and was estimated to be 436 ± 48, 375 ± 48, 775 ± 62, 365 ± 26, and 290 ± 53 J/m^2,
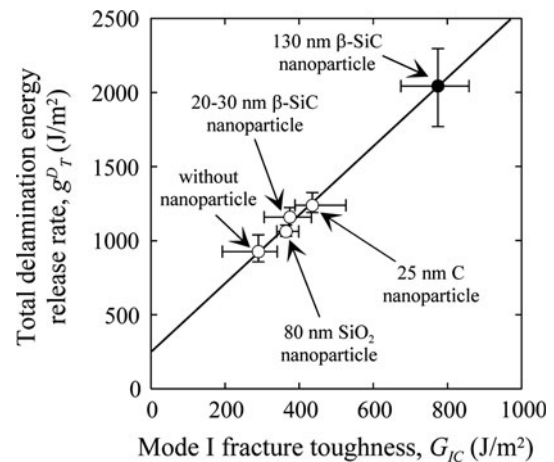

Fig. 9 Relation between the delamination-energy-release rate of hybrid carbon fiber/polyimide composites and the mode I fracture toughness of bulk polyimides

respectively.[6] Figure 9 shows the relation between the total delamination energy-release rate of hybrid carbon fiber/polyimide composites and mode I fracture toughness indicated by the energy-release rate of bulk polyimides. For hybrid carbon fiber/polyimide composites with 130 nm β-SiC nanoparticles, minor delamination-crack growth was observed, and the total delamination-energy-release rate was assumed to be 2044 ± 152 J/m^2, i.e., the critical total energy-release rate of the K13D fiber/polyimide composite. The total delamination-energy-release rate increased with the increasing mode I fracture toughness of bulk polyimide nanocomposites, and there is a linear relation between the total delamination-energy-release rate in hybrid carbon fiber/polyimide composites and the mode I fracture toughness of bulk polyimides.

The difference between the total delamination-energy-release rate of hybrid carbon fiber/polyimide composites and mode I fracture toughness of bulk polyimides is possibly attributed to mechanisms that contribute to toughness. The loading mode of delaminated hybrid carbon fiber/polyimide composites is the mixed mode. The component of mode II was affected by the delamination-energy-release rate of the hybrid carbon fiber/polyimide composites. Moreover, fiber bridging occurred in hybrid carbon fiber/polyimide composites. This mechanism was also affected by delamination-energy-release rate of hybrid carbon fiber/polyimide composites. It is important to consider materials' combinations (i.e., different fibers and base resins) and stacking sequence in hybrid carbon fiber/polyimide

---

[6] In our previous investigation [34], the natural crack at the tip of a notch was introduced by tapping the fresh blades. The natural cracks at the tip of a notch for a few bulk polyimides with nanoparticles were also produced using fatigue loading to check the procedure (tapping procedure), and G_{IC} of these bulk polyimides was similar to that obtained by tapping cracked bulk polyimides.

composites. In this study, the materials' combination and stacking sequence in hybrid carbon fiber/polyimide composites were the same, and delamination-energy-release rates were calculated using the average delamination crack length for each layer (the number of delaminations was not considered). When the stacking sequence of the hybrid carbon fiber/polyimide composites was changed from $[0_{(T1000GB)}/0_{(K13D)}]_{2S}$ to $[(0_{(T1000GB)})_2/(0_{(K13D)})_2]_S$, the number of delaminations decreased, and a different total delamination-energy-release rate was possibly observed. The fiber/matrix interface adhesion of hybrid carbon fiber/polymer composites, which is related to the combination of materials, is also important. The weak bonds between the fibers and matrix might cause an interfacial fracture without enhancing the delamination- energy-release-rate due to the addition of nanoparticles.

Concluding remarks

The tensile properties and fracture behavior of high-strength T1000GBPAN-based and high-modulus K13D pitch-based hybrid carbon fiber/polyimide composites with 25 nm C, 20–30 nm β-SiC, 130 nm β-SiC, 80 nm SiO$_2$, and 300 nm SiO$_2$ nanoparticles in the matrix were examined. For hybrid carbon fiber/polyimide composites with and without 25 nm C, 20–30 nm β-SiC, and 80 nm SiO$_2$ nanoparticles, the tensile stress–strain curve has a complex shape, and these hybrid carbon fiber/polyimide composites endure high stress without instantaneous failure. However, for hybrid carbon fiber/polyimide composites with 130 nm β-SiC and 300 nm SiO$_2$ nanoparticles, the tensile stress–strain curve shows brittle behavior. The selection of nanoparticles was critical in preventing an instantaneous failure. The initial failure strain in hybrid carbon fiber/polyimide composites with and without 25 nm C, 20–30 nm β-SiC, and 80 nm SiO$_2$ nanoparticles was higher than that in K13D fiber/polyimide composites; the final failure strain in hybrid carbon fiber/polyimide composites with and without these nanoparticles was similar to that of T1000GB fiber/polyimide composites. For hybrid carbon fiber/polyimide composites with and without these nanoparticles, the total delamination-energy-release rate estimated from the compliance method using holding stress that increased with increasing mode I fracture toughness obtained from bulk polyimide nanocomposites. In addition, there is a linear relation between the total delamination-energy-release rate of hybrid carbon fiber/polyimide composites and the mode I fracture toughness of bulk polyimides. The stress after the initial failure in hybrid carbon fiber/polyimide composites improved by adding these nanoparticles to the matrix and correlated with the mode I fracture toughness of the polyimide matrix.

References

1. Fitzer E (1989) Carbon 27(5):621. doi:10.1016/0008-6223(89)90197-8
2. Chand S (2000) J Mater Sci 35(6):1303. doi:10.1023/A:1004780301489
3. Bunsell AR, Harris B (1974) Composites 5(4):157. doi:10.1016/0010-4361(74)90107-4
4. Summerscales J, Short D (1978) Composites 9(3):157. doi:10.1016/0010-4361(78)90341-5
5. Aveston J, Kelly A (1980) Philos T R Soc A 294(1411):519. doi:10.1098/rsta.1980.0061
6. Hayashi T, Koyama K, Yamazaki A, Kihira M (1972) Fukugo Zairyo (composite materials) 1:21
7. Short D, Summerscales J (1979) Composites 10(4):215. doi:10.1016/0010-4361(79)90022-3
8. Short D, Summerscales J (1980) Composites 11(1):33. doi:10.1016/0010-4361(80)90019-1
9. Hardaker KM, Richardson MOW (1980) Polym-Plast Technol 15(2):169. doi:10.1080/03602558008070011
10. Chow TW, Kelly A (1980) Ann Rev Mater Sci 10:229. doi:10.1146/annurev.ms.10.080180.001305
11. Morgan P (2005) Properties of carbon fibers. In: Morgan P (ed) Carbon fibers and their composites. Taylor, New York, p 791
12. Huang Y, Young RJ (1995) Carbon 33(2):97. doi:10.1016/0008-6223(94)00109-D
13. Paris O, Loidl D, Peterlik H (2002) Carbon 40(4):551. doi:10.1016/S0008-6223(01)00139-7
14. Naito K, Tanaka Y, Yang JM, Kagawa Y (2008) Carbon 46(2):189. doi:10.1016/j.carbon.2007.11.001
15. Naito K, Tanaka Y, Yang JM, Kagawa Y (2009) J Am Ceram Soc 92(1):186. doi:10.1111/j.1551-2916.2008.02868.x
16. Naito K, Yang JM, Tanaka Y, Kagawa Y (2012) J Mater Sci 47(2):632. doi:10.1007/s10853-011-5832-x
17. Landis AL, Lau KSY (1998) In: Goodman SH (ed) Handbook of thermoset plastics, 2nd edn. Noyes, New Jersey, p 302
18. Sroog CE (1996) In: Ghosh MK, Mittal KL (eds) Polyimides: fundamentals and applications. Dekker, New York, p 1
19. Bekyarova E, Thostenson ET, Yu A, Kim H, Gao J, Tang J, Hahn HT, Chou TW, Itkis ME, Haddon RC (2007) Langmuir 23(7):3970. doi:10.1021/la062743p
20. Hussain M, Nakahira A, Niihara K (1996) Mater Lett 26(3):185. doi:10.1016/0167-577X(95)00224-3
21. Timmerman JF, Hayes BS, Seferis JC (2002) Compos Sci Technol 62(9):1249. doi:10.1016/S0266-3538(02)00063-5
22. Siddiqui NA, Woo RSC, Kim JK, Leung CCK, Munir A (2007) Compos Part A-Appl S 38(2):449. doi:10.1016/j.compositesa.2006.03.001
23. Xu Y, Van Hoa S (2008) Compos Sci Technol 68(3–4):854. doi:10.1016/j.compscitech.2007.08.013
24. Thostenson ET, Li WZ, Wang DZ, Ren ZF, Chou TW (2002) J Appl Phys 91(9):6034. doi:10.1063/1.1466880
25. Yokozeki T, Iwahori Y, Ishiwata S (2007) Compos Part A-Appl S 38(3):917. doi:10.1016/j.compositesa.2006.07.005
26. Iwahori Y, Ishiwata S, Sumizawa T, Ishikawa T (2005) Compos Part A-Appl S 36(10):1430. doi:10.1016/j.compositesa.2004.11.017
27. Arai M, Noro Y, Sugimoto K, Endo M (2008) Compos Sci Technol 68(2):516. doi:10.1016/j.compscitech.2007.06.007

28. Yang Y, Lu CX, Su XL, Wang XK (2007) J Mater Sci 42(15):6347. doi:10.1007/s10853-006-1198-x

29. Cho J, Chen JY, Daniel IM (2007) Scr Mater 56(8):685. doi:10.1016/j.scriptamat.2006.12.038

30. Jiang ZY, Zhang H, Zhang Z, Murayama H, Okamoto K (2008) Compos Part A-Appl S 39(11):1762. doi:10.1016/j.compositesa.2008.08.005

31. Ogasawara T, Ishida Y, Kasai T (2009) Compos Sci Technol 69(11–12):2002. doi:10.1016/j.compscitech.2009.05.003

32. MSDS of skybond 703 polyimide resin (1996) Industrial Summit Technology Co., Shenzhen

33. ASTM D792-08 (2009) In: ASTM annual book of standards, vol 08.01. American Society for Testing and Materials, West Conshohocken. doi:10.1520/D0792-08

34. Naito K, Yang JM, Kagawa Y (2011) Mat Sci Eng A-Struct 530:357. doi:10.1016/j.msea.2011.09.096

35. Zhou YX, Pervin F, Rangari VK, Jeelani S (2006) Mat Sci Eng A-Struct 426(1–2):221. doi:10.1016/j.msea.2006.04.031

36. ASTM D3171-11 (2011) In: ASTM annual book of standards, vol 15.03. American Society for Testing and Materials, West Conshohocken. doi:10.1520/D3171-11

37. Saunders RA, Lekakou C, Bader MG (1999) Compos Sci Technol 59(7):933. doi:10.1016/S0266-3538(98)00137-7

38. Thomason JL (1995) Composites 26(7):467. doi:10.1016/0010-4361(95)96804-F

39. Marom G, Fischer S, Tuler FR, Wagner HD (1978) J Mater Sci 13(7):1419. doi:10.1007/BF00553194

40. Stevanovic MM, Stecenko TB (1992) J Mater Sci 27(4):941. doi:10.1007/BF01197646

41. Yao L, Li WB, Wang N, Li W, Guo X, Qiu YP (2007) J Mater Sci 42(16):6494. doi:10.1007/s10853-007-1534-9

42. Kretsis G (1987) Composites 18(1):13. doi:10.1016/0010-4361(87)90003-6

43. You YJ, Park YH, Kim HY, Park JS (2007) Comps Struct 80(1):117. doi:10.1016/j.compstruct.2006.04.065

44. Tada H, Paris PC, Irwin GR (2000) In: Tada H, Paris PC, Irwin GR (eds) The stress analysis of cracks handbook, 3rd edn. The American Society of Mechanical Engineers (ASME), New York, p 487. doi:10.1115/1.801535.fm

45. Hwang SF, Shen BC (1999) Compos Sci Technol 59(12):1861. doi:10.1016/S0266-3538(99)00047-0

46. Naito K, Yang JM, Kagawa Y (2012) J Mater Sci 47(6):2743. doi:10.1007/s10853-011-6101-8